Published in "Journal of Physics D: Applied Physics 49(37): 375201, 2016"
which should be cited to refer to this work.

Electron attachment properties of c-C_4F_8O in different environments

A Chachereau[1], J Fedor[2], R Janečková[3,4], J Kočišek[2], M Rabie[1] and C M Franck[1]

[1] Power Systems and High Voltage Laboratories, ETH Zurich, CH-8092 Zurich, Switzerland
[2] J. Heyrovský Institute of Physical Chemistry, Czech Academy of Sciences, Dolejškova 3, CZ-18223 Prague, Czech Republic
[3] Department of Chemistry, University of Fribourg, Chemin du Musée 9, CH-1700 Fribourg, Switzerland
[4] Faculty of Safety Engineering, VŠB—Technical University of Ostrava, Lumírova 13, CZ-70030, Ostrava 3—Výškovice, Czech Republic

E-mail: alisec@ethz.ch (A Chachereau) and juraj.fedor@jh-inst.cas.cz (J Fedor)

Abstract

The electron attachment properties of octafluorotetrahydrofuran (c-C_4F_8O) are investigated using two complementary experimental setups. The attachment and ionization cross sections of c-C_4F_8O are measured using an electron beam experiment. The effective ionization rate coefficient, electron drift velocity and electron diffusion coefficient in c-C_4F_8O diluted to concentrations lower than 0.6% in the buffer gases N_2, CO_2 and Ar, are measured using a pulsed Townsend experiment. A kinetic model is proposed, which combines the results of the two experiments.

Keywords: C_4F_8O, octafluorotetrahydrofuran, attachment cross section, swarm parameters, three-body attachment

Introduction

Octafluorotetrahydrofuran (c-C_4F_8O) is considered for use as a radiating medium in Cherenkov detectors [1] and as a cleaning agent for chemical vapor deposition chambers to replace plasma processing gases with high global warming potential (GWP) [2]. The GWP of c-C_4F_8O is about 8000 [2]. It could also be considered as an alternative to sulphur hexafluoride (SF_6) in high voltage gaseous insulation. SF_6 has a high dielectric strength, low boiling point and chemical stability, but it has a GWP of 23 500 [3]. Therefore, it could be advantageously replaced by diluted mixtures of c-C_4F_8O with one or more buffer gases, such as N_2 or CO_2.

Electron swarm parameters such as the effective ionization rate, the electron drift velocity and the electron diffusion coefficient are useful for modeling low temperature plasmas in general [4, 5], and in particular for modelling non-thermal gas discharges and assessing the performance of an electronegative gas for high voltage insulation [6, 7]. It is common practice to calculate the effective ionization rate by solving the electron Boltzmann equation [8], or by means of Monte-Carlo simulations [9, 10]. The required electron scattering cross sections can be obtained for instance by means of electron beam experiments [11]. However, the ion kinetic processes are often neglected in such models, since it would require considerable effort to determine the scattering cross sections of ions and to calculate the transport properties of both electrons and ions. This is problematic in some electronegative gases where electron attachment proceeds through the formation of an unstable parent anion, and the collisions of this anion with neutrals are crucial for the electron attachment rate [12, 13]. Another approach is to measure the effective ionization rate in a swarm experiment [14]. The effective ionization rate coefficient resulting from all kinetic processes is obtained, but less information is gained on the kinetic scheme itself. Therefore, the two approaches are complementary. Finally, since both beam and swarm experiments are performed in specific conditions, typically at low gas pressures, and for a limited number of gas

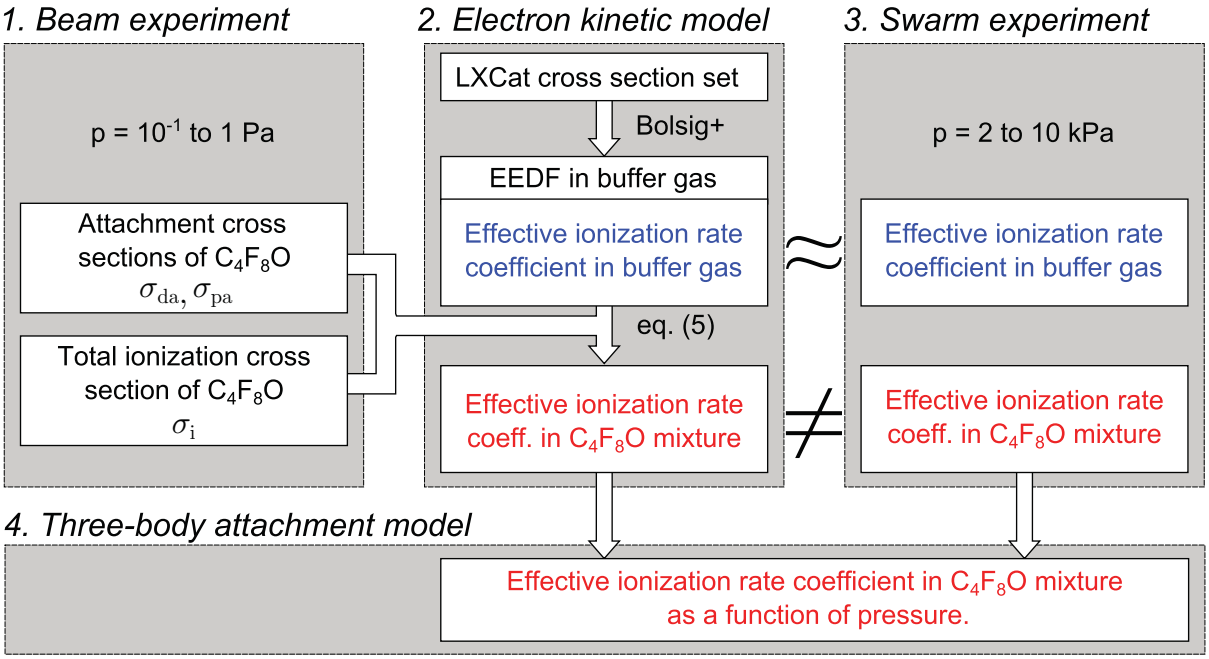

Figure 1. Structure of the paper and overview of the measurements and calculations. 'EEDF' stands for electron energy distribution function, 'p' stands for gas pressure.

mixtures, kinetic models are necessary to extend this data to other conditions, such as the high gas pressures of several bar used in high voltage insulation equipment.

In the present work, the properties of c-C_4F_8O are investigated in two different environments: pure c-C_4F_8O at low gas pressure in an electron beam experiment, and diluted mixtures of c-C_4F_8O in N_2, CO_2 and Ar at intermediate gas pressure in a swarm experiment. The results are combined to propose a model for electron attachment to c-C_4F_8O. The structure of this work is shown in figure 1. In section 1, the attachment cross sections and the total ionization cross section of c-C_4F_8O are obtained using an electron beam experiment. In section 2, the electron Boltzmann equation is solved in the buffer gases N_2, CO_2 and Ar to obtain the electron energy distribution function, the electron drift velocity and the effective ionization rate. It is discussed how the attachment and ionization processes in c-C_4F_8O identified in the beam experiment can be used for calculating the effective ionization rate in c-C_4F_8O mixtures with N_2, CO_2 and Ar. Then, the effective ionization rate is calculated in the mixtures of 0.5% c-C_4F_8O in CO_2, 0.6% c-C_4F_8O in N_2 and 0.1% c-C_4F_8O in Ar. In section 3, the electron swarm parameters are measured in N_2, CO_2 and Ar and in the aforementioned mixtures with c-C_4F_8O, at different gas pressures, using a pulsed Townsend experiment. Swarm parameters measurements in similar mixtures were presented in a previous work [15], however, these measurements were limited to a narrower pressure range and the pressure dependence of results was not investigated. As the results from sections 2 and 3 are found to be conflicting, a three-body attachment mechanism is proposed in section 4 to complete the electron kinetics scheme described in section 2. This model is consistent with the two experiments, and useful for extending the present data to arbitrary gas pressures and small concentrations of c-C_4F_8O.

1. Beam experiment

1.1. Experimental setup

In the first experimental setup—a quantitative dissociative electron attachment (DEA) spectrometer [16, 17]—the electron beam passes a stagnant gas target of c-C_4F_8O at single-collision conditions. The electrons emitted from a hot filament are selected according to their kinetic energy in a trochoidal electron monochromator. They are then accelerated to desired energy and pass through the collision chamber filled with the studied gas. The electron current is monitored by a Faraday cup located behind the collision cell.

The entire experiment is pulsed: the electrons pass the target chamber during 200 ns while it is field-free and after additional 200 ns (when the electrons leave the chamber) a negative voltage of −300 V is pulsed across the chamber which pushes the anions formed in the cell towards the ion time-of-flight (TOF) mass analyzer in the direction perpendicular to the electron beam. The anions are detected with a microchannel plate, counted, and their arrival times are analyzed. The time between anion production and their detection is in the order of microseconds, namely 7.6 μs for the heaviest anion in the present measurements. The experiment is repeated with 50 kHz frequency. The spectra are stored as two-dimensional maps—ion count as a function of electron energy and of arrival time. This allows the extraction of both negative ion mass spectra and ion-yield versus electron-energy for each anion.

The electron-energy scale is calibrated using the onset of O^- signal from CO_2 at 3.99 eV. The shape of the O^- peak is also used to determine the energy resolution of the electron beam as described in [18]. The absolute cross sections are calibrated using two independent reference values: the O^- from CO_2 [19]

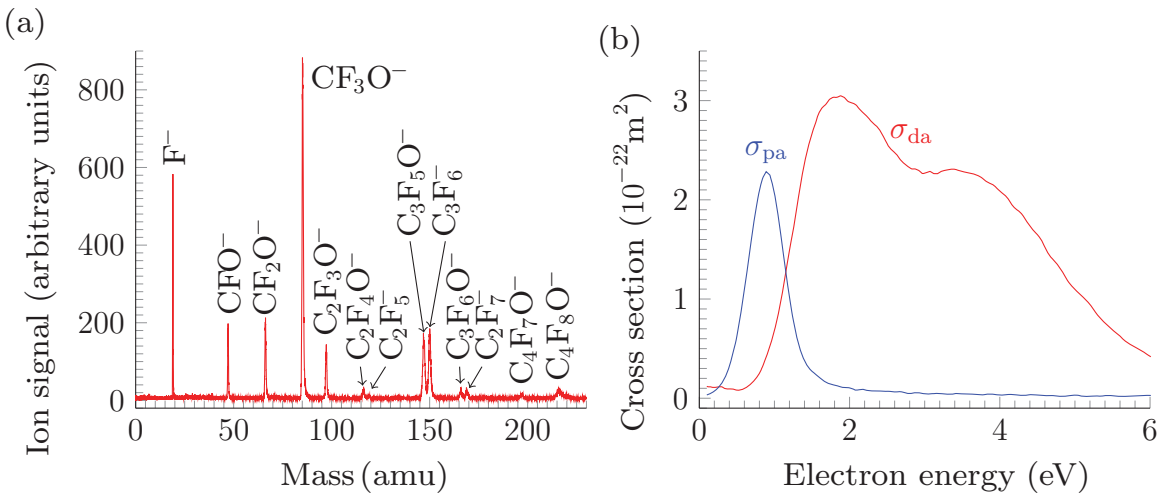

Figure 2. (a) Negative ion mass spectrum in the beam experiment recorded at an electron energy of 2 eV. (b) Total dissociative electron attachment cross section σ_{da} (sum of the partial cross sections for all the anionic fragments shown in (a)), and parent anion attachment cross section σ_{pa}.

and $HCOO^-$ from HCOOH [20]. The uncertainty of the obtained cross sections is ±20% (two standard deviations). It is obtained as a combination or the error of the present relative measurements (±15%) and of the error of the absolute cross sections used for normalization. The latter is taken as ±15% in view of the results from various groups listed in [20].

The electron-beam resolution in the current experiment is approximately 200 meV. As seen from test measurements with a small impurity of SF_6, the electrons down to the energy of approximately 100 meV are present in the beam. The pressure in the cell is monitored with a capacitance manometer and is varied from 1×10^{-2} to 1×10^{-1} Pa. This range of pressures ensures single-collision conditions between electrons and the gas molecules, and ensures that the collision probability of created anions with other molecules is negligible on timescale of the anion extraction.

Additionally to electron attachment cross sections, both dissociative and non-dissociative, the total positive ionization cross section has also been measured. For the purpose of this measurement, the setup was used in the total ion collection mode [19]. Here the monochromator is not pulsed and the total analogue ion current (in the order of picoamperes) is measured on the molybdenum electrode placed in the collision chamber. This is the same electrode that serves as a pusher in the pulsed mode. For the sake of the continuous wave measurements, it is connected to a picoampermeter. The ion current is recorded as a function of electron energy. The cross section is then calibrated by recording the ion current for argon which has known positive ionization cross section [21].

1.2. Ionization and attachment cross sections of c-C_4F_8O at single-collision conditions

Upon electron impact in the electron energy range up to 6 eV, the c-C_4F_8O molecule exhibits a rich fragmentation pattern. Figure 2(a) shows the negative ion mass spectrum recorded at the electron energy of 2 eV. A number of anionic fragments can be seen, which is expected for a molecular system of this size [18]. What is not expected, is the observation of the parent anion $C_4F_8O^-$. At single collision conditions, the process of electron attachment basically always proceeds via formation of the transient anion, also called a resonance, in this case $(C_4F_8O^-)^*$. The transient anion has an excess of internal energy which is released either by autodetachment of the electron on the timescale of typically femto- to picoseconds, or by anion's dissociation on the same timescale which leads to stable anionic fragments. In present case, however, some transient negative ions survive up to 7.6 μs, which is their detection time in the time-of-flight spectrometer.

Figure 2(b) shows the total dissociative electron attachment cross section σ_{da} (sum of partial cross sections for all the anionic fragments) and the cross section σ_{pa} for the production of the parent anion $(C_4F_8O^-)^*_L$ ('L' is standing for long-lived). The electron attachment cross sections show three peaks (one peak in σ_{pa} and two peaks in σ_{da}) which correspond to elementary attachment processes mediated by the formation of different types of transient anions. The peaks are positioned at 0.9, 1.8 and 3.4 eV. The first peak at 0.9 eV corresponds to the production of the long-lived parent anion $(C_4F_8O^-)^*_L$. It is produced at energies considerably higher than thermal, which is rare. Most of the known long-lived parent anions created in binary collisions with an electron are formed at energies close to 0 eV, e.g. SF_{6-} or CCl_{4-}. The stabilization mechanism of the $(C_4F_8O^-)^*_L$ on the microsecond time scale and its fragmentation pathways will be discussed in a separate publication [22]. The second and third peaks at 1.8 and 3.4 eV correspond to dissociative attachment processes.

In order to ensure that three-body mechanisms do not play a role in the beam experiment, a range of control measurements was performed. All ion yields—both of the fragmented anions and of the parent anion $(C_4F_8O^-)^*_L$—were found to be linearly dependent on the target gas pressure. Also, all signals were linearly dependent on the electron current passing the collision cell.

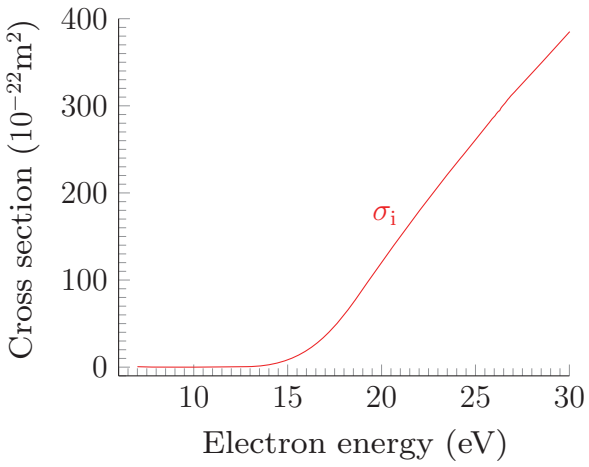

Figure 3. Total positive ionization cross section of c-C_4F_8O.

Figure 3 shows the total positive ionization cross section σ_i of c-C_4F_8O. Since the positive cross section is measured with the setup operated in the total ion collection mode, the partial cross sections are not available. This cross section was measured to provide an input for calculations of section 2, where only the total ionization cross section is needed. The ionization energy is 11.8 eV. It was determined by fitting the measured data by a Wannier-like threshold law [23, 24].

2. Electron kinetic model

In section 1, the total ionization and dissociative attachment cross sections, σ_i and σ_{da} were obtained, as well as the long-lived parent anion attachment cross section σ_{pa}. These scattering cross sections correspond to the kinetic processes (1)–(3)

$$C_4F_8O + e \xrightarrow{k_i} 2e + A^+ (+B) \text{ (all ionization processes)}, \quad (1)$$

$$C_4F_8O + e \xrightarrow{k_{da}} D^- + E \quad \text{(all dissociative attachment processes)}, \quad (2)$$

$$C_4F_8O + e \rightleftarrows k_{pa} \; (C_4F_8O^-)^*_L \quad \text{(parent ion attachment, long-lived)}. \quad (3)$$

In the above kinetic scheme, k_i, k_{da} and k_{pa} are the reaction rate coefficients for the processes of ionization, dissociative attachment, and long-lived parent ion formation. The rate coefficient k can be calculated from the corresponding scattering cross section σ as follows

$$k = \sqrt{\frac{2}{m_e}} \int_0^\infty \sigma \varepsilon f(E/N, \varepsilon) \mathrm{d}\varepsilon, \quad (4)$$

where m_e is the electron mass and $f(E/N, \varepsilon)$ is electron energy distribution function (EEDF) in the gas or gas mixture. The EEDF is obtained by solving the Boltzmann equation for electrons, which requires the input of the electron scattering cross sections for all the considered gases. Full cross section sets are available for N_2, CO_2 and Ar, for instance on the LXcat database [5, 25]. In this work, the cross section set from Biagi [26] is used for N_2, Phelps [27] for CO_2, and SIGLO [28] for Ar. A set of electron scattering cross sections for c-C_4F_8O is presently not available. However, it can be assumed that the EEDF in the buffer gas is not changed when a small amount of c-C_4F_8O is added [29, 30]. Therefore, the rate coefficients k_i, k_{da} and k_{pa} in the diluted c-C_4F_8O mixtures can be calculated using equation (4) and taking the EEDF calculated for the buffer gas.

The electron Boltzmann equation is solved using the solver Bolsig+ [8], which makes use of the two-term approximation, to obtain the EEDF, the effective ionization rate coefficient k^b_{eff}, the electron drift velocity w^b and the longitudinal electron diffusion coefficient ND^b_L in the buffer gases N_2, CO_2 and Ar. The present calculations are performed at relatively low density reduced electric field E/N (E is the electric field and N is the gas number density). In this range of E/N, the two-term approximation yields precise results, as was shown for instance in N_2 [31] and Ar [32].

The effective ionization rate coefficient k^0_{eff} (the exponent 0 is used later on in section 4 to signify 'limit at low pressure') in a diluted mixture of c-C_4F_8O with N_2, CO_2 or Ar can obtained as

$$k^0_{eff} = (1 - r)k^b_{eff} + r(k_i - k_{da} - k_{pa}), \quad (5)$$

where r is the ratio of c-C_4F_8O in the mixture.

In this model—processes (1)–(3)—electron detachment from $(C_4F_8O^-)^*_L$ is neglected. Autodetachment from $(C_4F_8O^-)^*_L$ is indeed negligible on the timescale of the swarm experiment since the lifetime of $(C_4F_8O^-)^*_L$ was found to be at least microseconds, but there is the possibility for collisional detachment in the swarm experiment. Therefore, the electron attachment via process (3) is possibly overestimated.

Using equation (5), k^0_{eff} is calculated in the mixtures of 0.6% c-C_4F_8O in N_2, 0.5% c-C_4F_8O in CO_2 and 0.1% c-C_4F_8O in Ar. The calculated values of k^b_{eff}, w^b and ND^b_L in the gases N_2, CO_2 and Ar and of k^0_{eff} in the corresponding gas mixtures are shown in figures 7–9, respectively, and compared to the same quantities measured in the swarm experiment.

3. Swarm experiment

3.1. Experimental setup and methods

The swarm parameter measurements were performed with the automated pulsed Townsend (PT) setup described in [33]. The experimental setup allows for varying the electrode gap distance, the voltage and the gas pressure. The measurements are performed at room temperature, which is monitored. About 10^7 electrons are released in the gas vessel from a 12 nm thick palladium photocathode, which is back illuminated by a 266 nm laser. The laser pulses have a duration of 1.5 ns FWHM and a 20 Hz repetition rate. The released electrons drift in an homogeneous electric field between two Rogowski profiled electrodes. Upon collision with sample gas molecules, ionization and attachment events lead to a growth or decrease of the

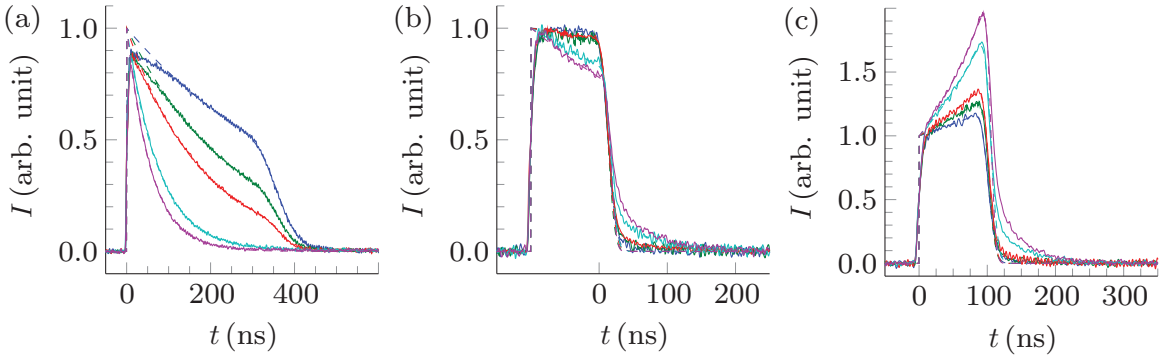

Figure 4. Current versus time in the mixture of 0.6% c-C_4F_8O in N_2 (a) for $E/N \simeq 26$ Td, (b) for $E/N \simeq 123$ Td and (c) for $E/N \simeq 137$ Td, at different gas pressures and for an electrode gap distance of 15 mm. In figure (a), the curves correspond from top to bottom to the pressures 2, 3, 4, 8 and 10 kPa, and the same color code is used in figures (b) and (c). The measured currents are in the range of 10–45 μA, they are here normalized so that the different curves have the same initial amplitude. The full lines are the measured currents, whereas the dashed lines correspond to fits of the analytical model (6).

electron swarm. The electrical displacement current across the gap is measured.

The electron swarm is modeled with a Gaussian spatial distribution of the electrons and the corresponding current can be expressed for $t \geqslant 0$ as [33]

$$I_e(t) = \frac{I_0}{2}\exp(\nu_{\text{eff}} t)\left(1 - \text{erf}\left(\frac{t - T_e}{\sqrt{2\tau_D t}}\right)\right), \quad (6)$$

$$I_0 = \frac{n_0 q_0}{T_e}, \quad (7)$$

where q_0 is the electron charge, I_0 is the electron current at time $t = 0$, T_e is the drift time and ν_{eff} is the effective ionization rate. The canonical error function 'erf' accounts for the absorption of the electrons at the anode. The characteristic time for longitudinal diffusion τ_D is related to the longitudinal diffusion coefficient D_L via $2D_L = w^2\tau_D$, where w is the electron drift velocity. The initial distribution of the electrons released by the laser is assumed to be a Dirac delta. The analytical model (6) is fitted to the measured current as described in detail in [34] to obtain the electron swarm parameters $k_{\text{eff}} = \nu_{\text{eff}}/N$, w and ND_L.

The measurements were performed in pure N_2, CO_2 and Ar, and in the mixtures of 0.6% c-C_4F_8O in N_2, 0.5% c-C_4F_8O in CO_2 and 0.1% c-C_4F_8O in Ar. The c-C_4F_8O has a purity of 99.5% (Linde), the Ar and N_2 have a purity of 6.0 and the CO_2 a purity of 5.0. The gases are filled into a vessel previously evacuated to a pressure of $\sim$1 Pa. The total gas pressure was varied from 2 to 10.5 kPa, the electrode gap distance from 11 to 17 mm, and the density reduced electric field E/N from 5 to 135 Td (1 Td $= 10^{-21}$ V · m^2).

3.2. Results

Sample current measurements in the mixtures of 0.6% c-C_4F_8O in N_2, 0.5% c-C_4F_8O in CO_2 and 0.1% c-C_4F_8O in Ar are shown in figures 4–6 respectively. The analytical model (6) fits well all the measured currents, except the falling edge of the measured current at 8 and 10 kPa in figures 4(b) and (c), which is discussed later.

The effective ionization rate coefficient k_{eff}, electron drift velocity w and longitudinal electron diffusion coefficient ND_L obtained experimentally in N_2, CO_2 and Ar, and in the corresponding mixtures are shown in figures 7–9. This data is also available on the LXcat website, ETHZ database [35].

3.3. Discussion

3.3.1. Measurements and calculations in the buffer gases. There is relatively good agreement between the measured effective ionization rate coefficient, electron drift velocity and density normalized longitudinal electron diffusion coefficient in pure N_2, CO_2 and Ar, and the same quantities calculated with Bolsig+ from the cross section sets [26–28]. The agreement is not perfect, but different cross section sets are available for these gases (see for instance the LXcat project [5]), and each set yields slightly different results. For instance the measured values in CO_2 are in between the calculated values using the cross sections sets [27] and [28] for CO_2 (the latter is not shown here). For the purpose of this work, the calculations from the sets [26–28] are in sufficiently good agreement with the measurements.

3.3.2. Measurements of w and ND_L in the c-C_4F_8O mixtures. In the mixture of 0.6% c-C_4F_8O in N_2, at the pressures of 8 and 10 kPa, a residual current is measured after the electron transit, as shown in figures 4(b) and (c) for times $t \geqslant 110$ ns. The falling edge of the waveform is asymmetrical, which indicates that the spatial distribution of electrons is not Gaussian. This asymmetrical broadening of the electron swarm could be due to delayed electrons, produced for instance via electron detachment from negative ions. Since the broadening of the swarm is different in the forward and backward directions, and is affected by another process than diffusion, the electron diffusion coefficient cannot be derived for these waveforms. Approximate values for the drift velocity at 8 and 10 kPa are shown in figure 7(c). The electron drift velocity w measured in the mixture of 0.6% c-C_4F_8O in N_2 seems slightly lower than the measured and calculated velocities in pure N_2, although it is still within the measurement error. The diffusion coefficient ND_L measured in the mixture of 0.6% c-C_4F_8O in

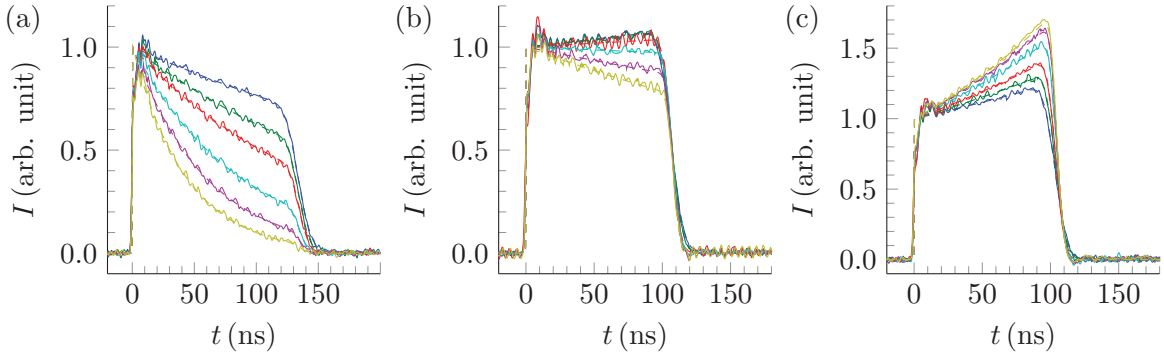

Figure 5. Current versus time in the mixture of 0.5% c-C_4F_8O in CO_2 (a) for $E/N \simeq 55$ Td, (b) for $E/N \simeq 99$ Td and (c) for $E/N \simeq 105$ Td, at different gas pressures and for an electrode gap distance of 15 mm. In figure (a), the curves correspond from top to bottom to the pressures 2, 3, 4, 6, 8 and 10 kPa, and the same color code is used in figures (b) and (c). The measured currents are in the range of 15–40 μA, they are here normalized so that the different curves have the same initial amplitude. The full lines are the measured currents, whereas the dashed lines correspond to fits of the analytical model (6).

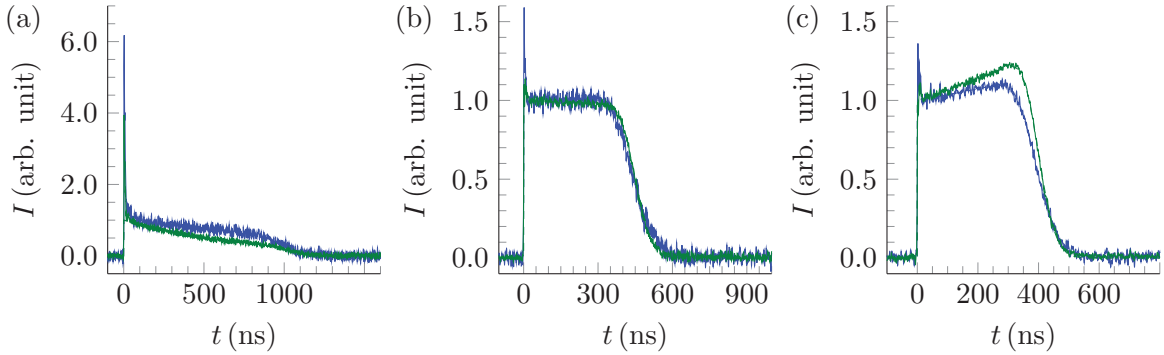

Figure 6. Current versus time in the mixture of 0.1% c-C_4F_8O in Ar (a) for $E/N \simeq 6$ Td, (b) for $E/N \simeq 26$ Td and (c) for $E/N \simeq 30$ Td, at different gas pressures and for an electrode gap distance of 11 mm. In figure (a), the curves correspond from top to bottom to the pressures 5 and 10 kPa, and the same color code is used in figures (b) and (c). The measured currents are in the range of 5 to 20 μA, they are here normalized so that the different curves have the same initial amplitude. The full lines are the measured currents, whereas the dashed lines correspond to fits of the analytical model (6).

N_2 is slightly larger than the measured and calculated ND_L in pure N_2.

The measured w and ND_L in the mixture of 0.5% c-C_4F_8O in CO_2 agree very well with the measured w and ND_L in pure CO_2 as shown in figures 8(b) and (c).

In the mixture of 0.1% c-C_4F_8O in Ar, in the range $E/N < 10$ Td, w strongly deviates from the measured and calculated values of w in pure Ar shown in figure 9(b). Such a change in w indicates a change of EEDF in the mixture. This makes the calculation of k_{eff}^0 in the c-C_4F_8O/Ar mixture in section 2 less reliable. The same effect was observed in [36] for small admixtures about 0.5% of octafluorocyclobutane c-C_4F_8 in Ar. This decrease of the drift velocity, often referred to as negative differential mobility or negative differential conductivity, has been studied extensively [37–39] and is considered common for diluted mixtures of molecular gases in Ar.

3.3.3. Measurements and calculations of k_{eff} in the c-C_4F_8O mixtures. The measurements of k_{eff} show that the addition of small amounts of c-C_4F_8O in N_2, CO_2 and Ar strongly decreases k_{eff}, and thus increases the density reduced critical electrical field $(E/N)_{\text{crit}}$ for which $k_{\text{eff}} = 0$. This increase of $(E/N)_{\text{crit}}$ is advantageous for electrical insulation applications. In all three mixtures the calculated values of k_{eff}^0 from section 2 clearly do not agree with the measured values of k_{eff}. They differ by approximately a factor of 5. Moreover, a strong pressure dependency of k_{eff} is observed in the c-C_4F_8O/N_2 and c-C_4F_8O/CO_2 mixtures. Since the electron kinetics scheme (1)–(3) obtained with the beam experiment fails to explain the swarm results, a model including three-body electron attachment is introduced in section 4.

4. Three-body attachment model

The importance of the density of the gaseous media on electron attachment is well known [13]. Complex molecules such as c-C_4F_8O, when capturing a free electron, can form a large number of unstable negative-ion states, also called parent anions. Parent ions have typically short autodetachment times due to their excess energy, but they can be stabilized upon collision with another molecule. In the beam experiment, due to the low pressure of the gas target, the ion-neutral collision timescale is about 10^{-4} s, and the anion extraction time is about 10^{-6} s. The collisional stabilization of parent ions is therefore negligible, and only stable anions and long-lived (mean autodetachment time $>10^{-6}$ s) parent anions are detected. In swarm experiments however, the collisions occur on the sub-nanosecond timescale, so that short-lived parent anions

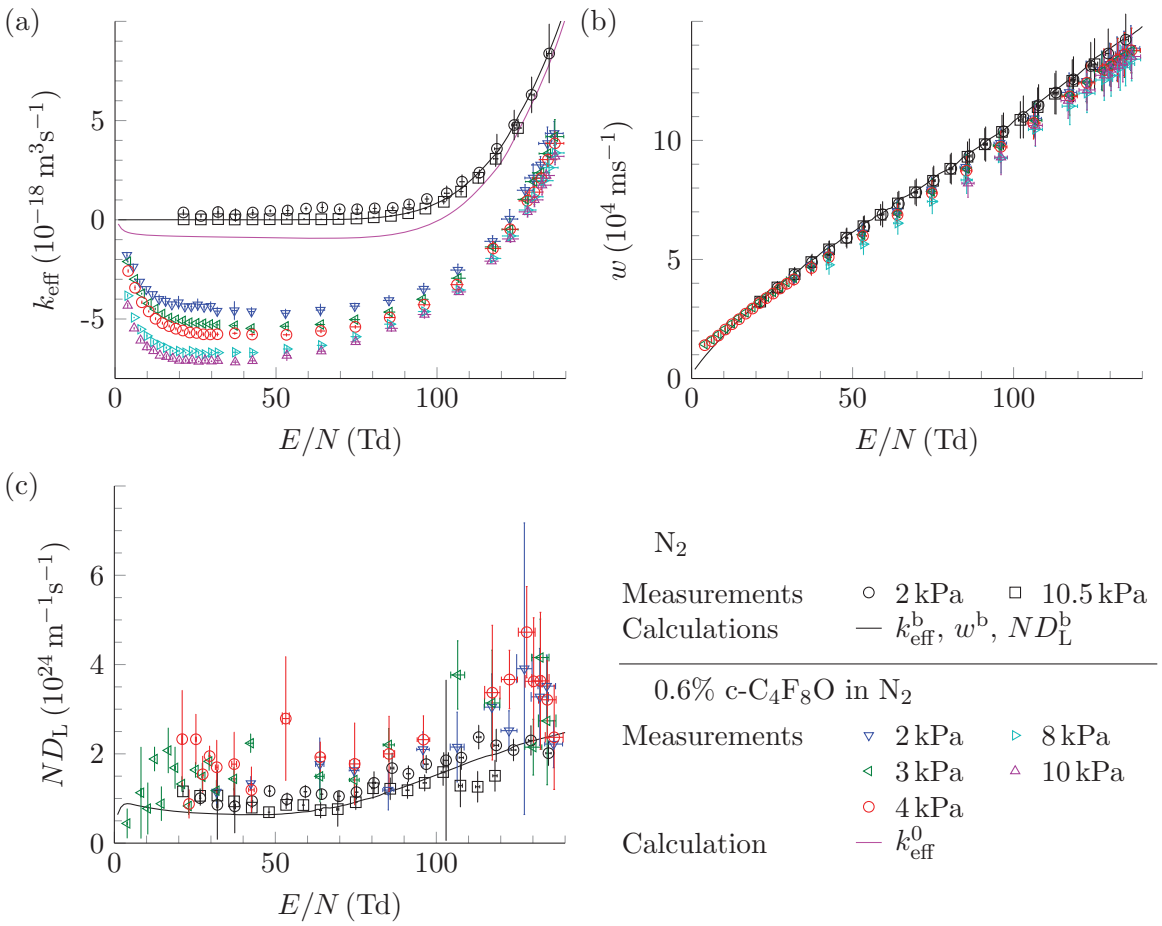

Figure 7. (a) Effective ionization rate coefficient, (b) electron drift velocity and (c) density normalized longitudinal electron diffusion coefficient versus E/N in N_2 and in the mixture of 0.6% c-C_4F_8O in N_2. Markers are measured values at different gas pressures, lines are calculated as indicated in section 2.

can significantly contribute to electron attachment via a three-body attachment mechanism. Furthermore, as the stabilization time depends on the gas pressure, three-body attachment results in a pressure dependence of k_{eff}.

4.1. Three-body attachment mechanism

In this model, additionally to the electron kinetic processes discussed in section 2, it is assumed that one additional unstable negative-ion state is formed, with an autodetachment time too short to be detected in the beam experiment but sufficiently long to allow stabilization in the swarm experiment. This short-lived parent anion, will be noted in the following $(C_4F_8O^-)^*_S$. Three-body attachment can be described by the processes

$$C_4F_8O + e \underset{\tau^{-1}}{\overset{k_{\mathrm{at}}}{\rightleftarrows}} (C_4F_8O^-)^*_S \qquad (8)$$

(parent ion attachment, short-lived),

$$(C_4F_8O^-)^*_S + M \overset{k_{\mathrm{stab}}}{\rightarrow} C_4F_8O^- + M \qquad (9)$$

(collisional stabilization),

$$(C_4F_8O^-)^*_S + M \overset{k_{\mathrm{det}}}{\rightarrow} e + C_4F_8O + M \qquad (10)$$

(collisional detachment).

In the above mechanism, k_{at} is the rate coefficient of $(C_4F_8O^-)^*_S$ formation, τ is the lifetime of $(C_4F_8O^-)^*_S$ towards autodetachment, k_{stab} is the rate coefficient for collisional stabilization of $(C_4F_8O^-)^*_S$ by a buffer gas molecule M, and k_{det} is the rate coefficient of electron detachment from $(C_4F_8O^-)^*_S$ upon collision with buffer gas molecule M. Since it is not *a priori* known at which electron energy this short-lived parent ion is formed, the channel (8) is considered distinct from the dissociative attachment channels.

The mechanism (1)–(3) and (8)–(10) corresponds to a system of differential equations for the densities of electrons and ions. Through the processes (8)–(10), the density of electrons is coupled with that of $(C_4F_8O^-)^*_S$. After a few τ, the growth of the electron number is exponential, with the rate [34, 40]

$$\nu_{\mathrm{eff}}(N) = k^{\mathrm{b}}_{\mathrm{eff}}[M] + (k_{\mathrm{i}} - k_{\mathrm{da}} - k_{\mathrm{pa}})[C_4F_8O] - \frac{k_{\mathrm{at}}k_{\mathrm{stab}}\tau[C_4F_8O][M]}{1 + \tau(k_{\mathrm{det}} + k_{\mathrm{stab}})[M]}. \qquad (11)$$

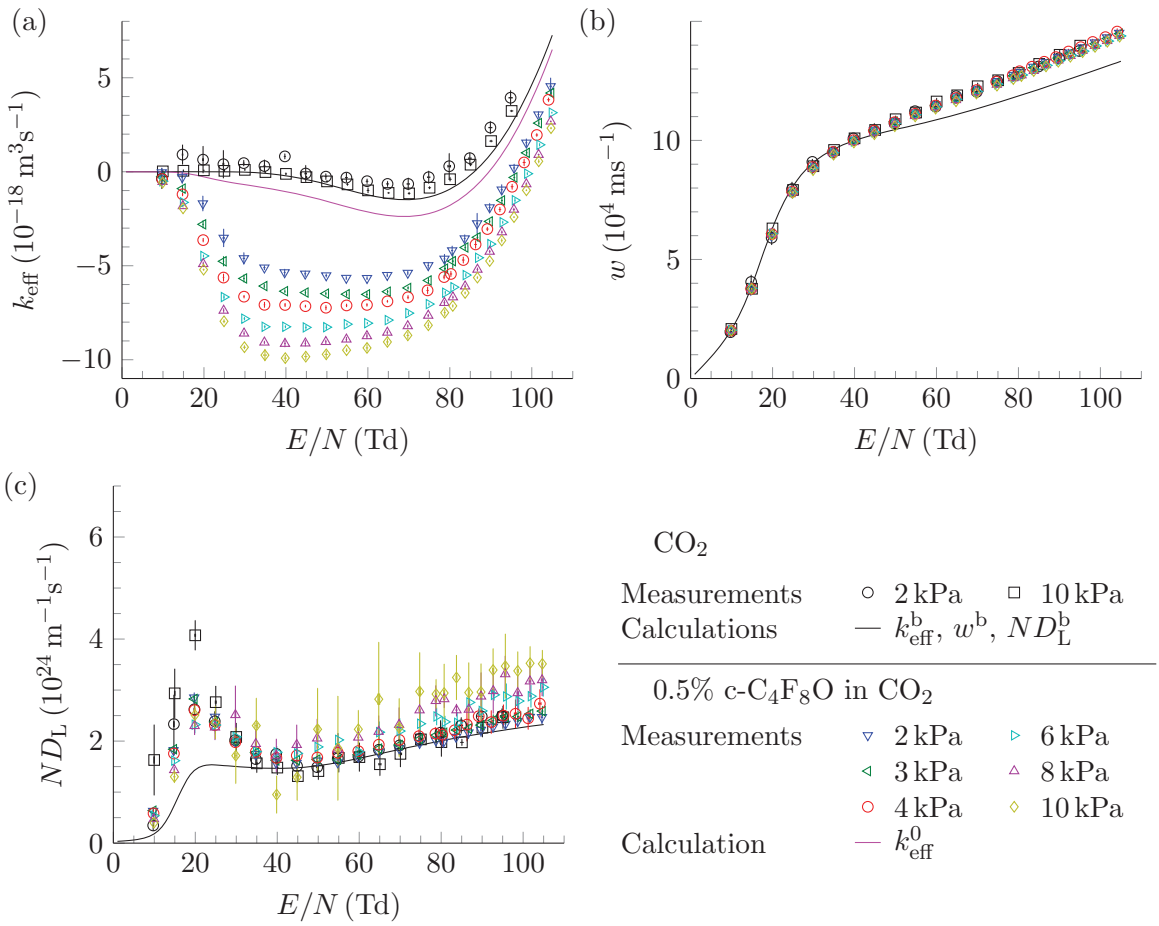

Figure 8. (a) Effective ionization rate coefficient, (b) electron drift velocity and (c) density normalized longitudinal electron diffusion coefficient versus E/N in CO_2 and in the mixture of 0.5% c-C_4F_8O in CO_2. Markers are measured values at different gas pressures, lines are calculated as indicated in section 2.

The number concentrations [M] and [C_4F_8O] can be expressed as a function of the total gas number density N and the ratio r of c-C_4F_8O

$$[\mathrm{M}] = (1 - r)N, \tag{12}$$

$$[\mathrm{C_4F_8O}] = rN. \tag{13}$$

We recognize the term $k^{\mathrm{b}}_{\mathrm{eff}}[\mathrm{M}] + (k_{\mathrm{i}} - k_{\mathrm{da}} - k_{\mathrm{pa}})[\mathrm{C_4F_8O}] = k^0_{\mathrm{eff}}(r)N$ calculated in section 2. Since we consider small ratios ($r \ll 1$) of c-C_4F_8O, we make the simplification

$$[\mathrm{M}] \approx N. \tag{14}$$

Furthermore, in the following we use the notations

$$k_{\mathrm{quad}} = k_{\mathrm{at}} k_{\mathrm{stab}} \tau, \tag{15}$$

$$N_{\mathrm{sat}} = ((k_{\mathrm{stab}} + k_{\mathrm{det}})\tau)^{-1}, \tag{16}$$

$$k_{\mathrm{sat}} = k_{\mathrm{quad}} N_{\mathrm{sat}}. \tag{17}$$

Adopting the above notations, equation (11) becomes

$$\nu_{\mathrm{eff}}(N) = k^0_{\mathrm{eff}}(r)N - \frac{k_{\mathrm{quad}} r N^2}{1 + N/N_{\mathrm{sat}}}. \tag{18}$$

The effective ionization rate ν_{eff} is a strong function of the gas density N in the experiment. By comparing N to N_{sat}, two limiting cases can be identified [40]

(i) When $N \ll N_{\mathrm{sat}}$, equation (18) simplifies as

$$\nu_{\mathrm{eff}}(N) = k^0_{\mathrm{eff}}(r)N - k_{\mathrm{quad}} r N^2, \tag{19}$$

and the three-body attachment rate increases quadratically with the gas density.

(ii) When $N \gg N_{\mathrm{sat}}$, equation (18) simplifies as

$$\nu_{\mathrm{eff}}(N) = k^0_{\mathrm{eff}}(r)N - k_{\mathrm{sat}} r N, \tag{20}$$

and the three-body attachment rate increases linearly with the gas density.

Thus, the quantity N_{sat} can be seen as a 'saturation' density for three-body attachment.

4.2. Rate coefficients and saturation density for three-body attachment to c-C_4F_8O

The simple model for the three-body electron attachment to c-C_4F_8O described in section 4.1 enables us to quantitatively characterize the kinetic processes (8)–(10) by determining N_{sat}, k_{sat} and k_{quad}.

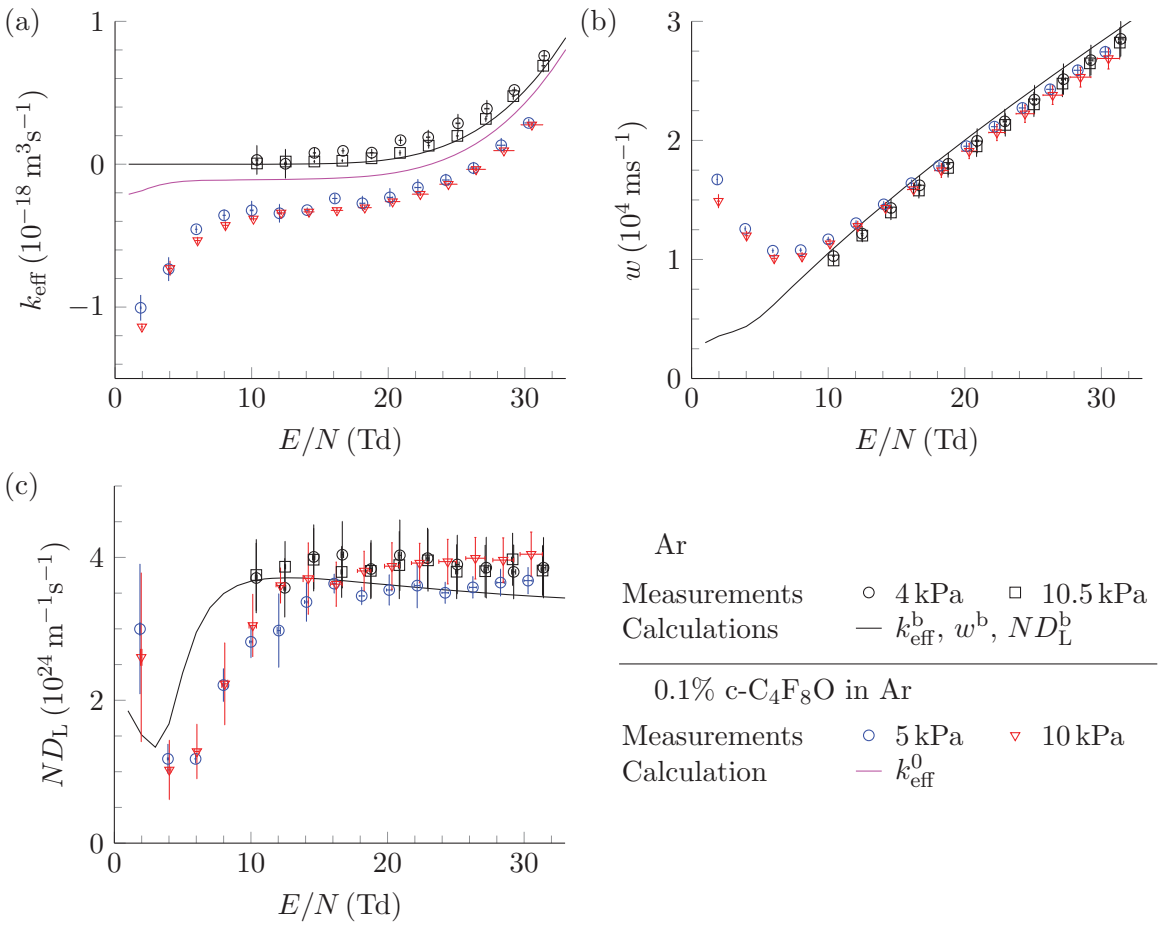

Figure 9. (a) Effective ionization rate coefficient, (b) electron drift velocity and (c) density normalized longitudinal electron diffusion coefficient versus E/N in Ar and in the mixture of 0.1% c-C_4F_8O in Ar. Markers are measured values at different gas pressures, lines are calculated as indicated in section 2.

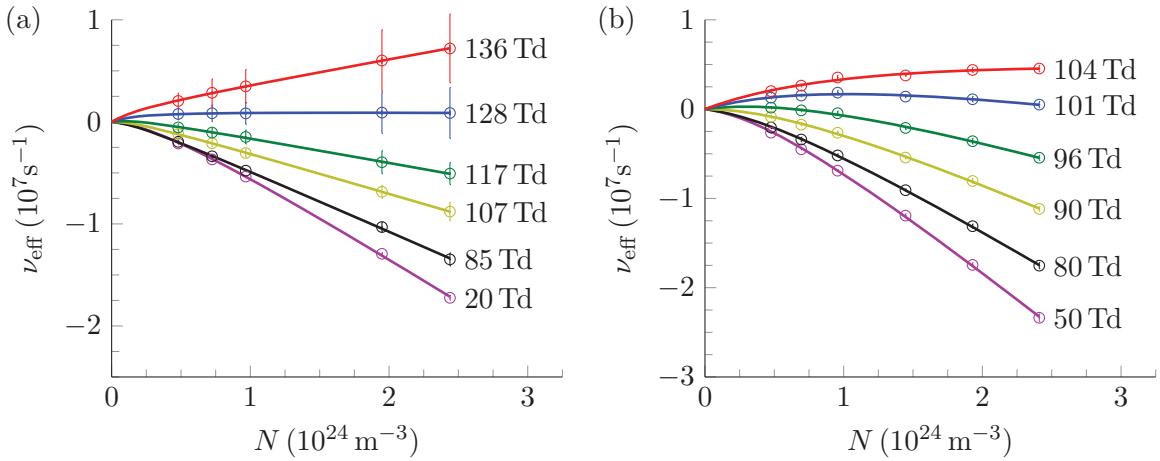

Figure 10. ν_{eff} as a function of N (a) in the c-C_4F_8O/N_2 mixture for sample E/N values between 20 and 135 Td and (b) in the c-C_4F_8O/CO_2 mixture for sample E/N values between 50 and 104 Td. Markers are measured values of ν_{eff}, and lines are fits with equation (18).

For measurements in the c-C_4F_8O/N_2 and c-C_4F_8O/CO_2 mixtures, the observed dependency of $\nu_{\mathrm{eff}}(N)$ corresponds not to either limiting cases (i) and (ii) but to the general case (18), where N_{sat} may be of the same order of magnitude as N ($N_{\mathrm{sat}} \sim N$). Therefore k_{quad} and N_{sat} are directly obtained from the fit of equation (18) to the measured $\nu_{\mathrm{eff}}(N)$. The rate coefficient k_{sat} is obtained simultaneously as the product $k_{\mathrm{quad}}N_{\mathrm{sat}}$ from equation (17). Examples of the fit of equation (18) on the measured $\nu_{\mathrm{eff}}(N)$ are shown in figure 10(a) for the N_2 mixture and in figure 10(b) for the CO_2 mixture.

In the c-C_4F_8O/Ar mixture, the measured k_{eff} is independent from the gas density. Normally, this could be interpreted as the absence of three-body attachment, but k_{eff} is much lower than k_{eff}^{0} calculated with the electron kinetics scheme from

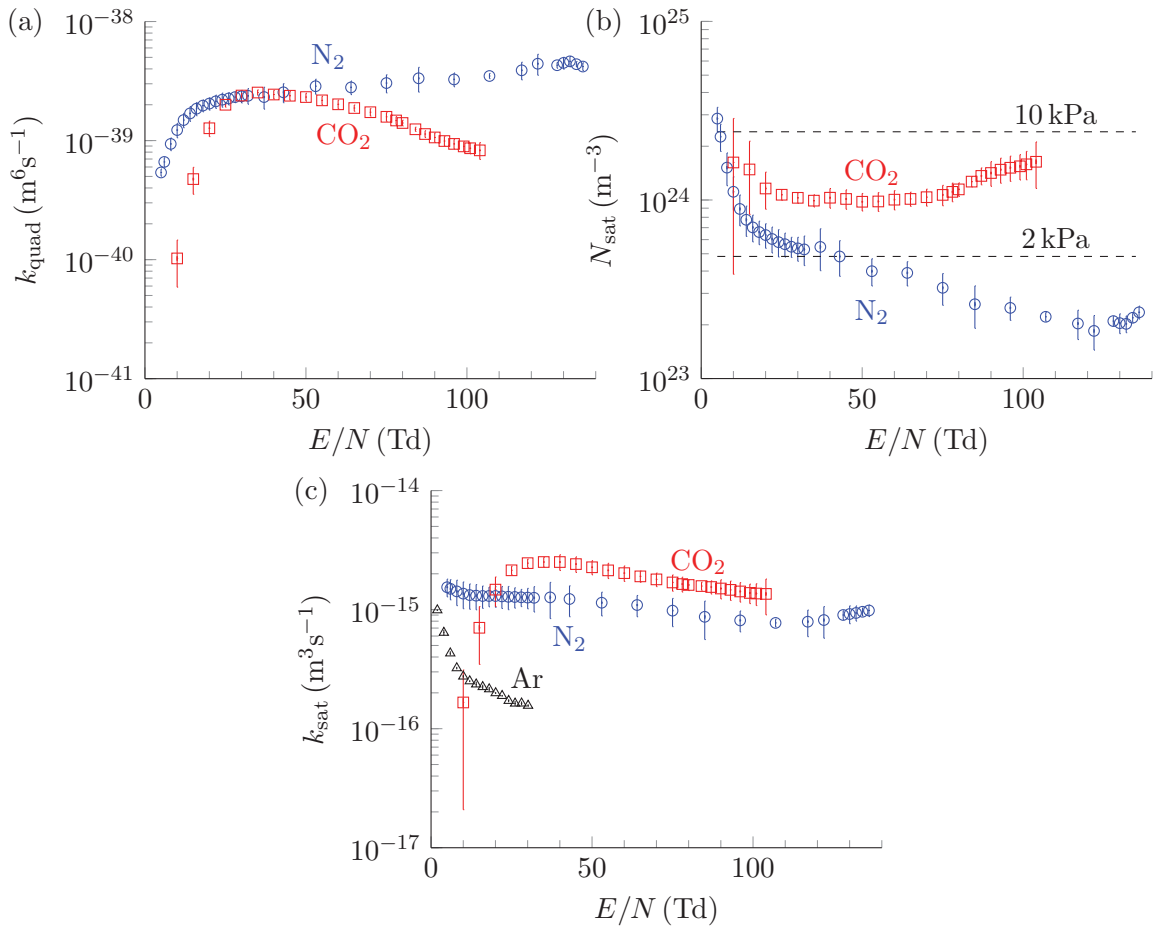

Figure 11. (a) Quadratic three-body attachment rate coefficient k_{quad}, (b) density of saturation N_{sat} and (c) saturated three-body attachment rate coefficient k_{sat} as a function of E/N in N_2 and CO_2.

section 2. Thus, the measurements in the c-C_4F_8O/Ar mixture correspond rather to the regime of saturated three-body attachment (ii). In this case, the saturated three-body attachment rate coefficient k_{sat} can be obtained as $(k^0_{\mathrm{eff}} - k_{\mathrm{eff}})/r$ from equation (20). However, the calculation of k^0_{eff} in the c-C_4F_8O/Ar mixture is probably imprecise, because the drift velocity measured in the c-C_4F_8O/Ar mixture indicates that the EEDF deviates from the EEDF of pure Argon, as mentioned in section 3.3.

The quadratic three-body attachment rate coefficient k_{quad}, the saturation density N_{sat} and the saturated three-body attachment rate coefficient k_{sat} in the c-C_4F_8O/N_2 and c-C_4F_8O/CO_2 mixtures are shown in figure 11. The saturation density N_{sat} is of the same order of magnitude as the gas density in the swarm experiment.

Interestingly, since the swarm measurements in the c-C_4F_8O/N_2 and c-C_4F_8O/CO_2 mixtures were performed in the pressure range where $N_{\mathrm{sat}} \sim N$, it was possible to identify both k_{quad} and N_{sat}. This makes it possible to calculate k_{eff} at at arbitrary gas pressure (provided that the pressure of c-C_4F_8O stays below its vapor pressure) and arbitrary low concentrations of c-C_4F_8O ($r \ll 1$) in the buffer gases N_2 and CO_2 using equation (18). In particular the limit of $k_{\mathrm{eff}}(N)$ at low gas pressure is given by $k^0_{\mathrm{eff}}(r)$ and the limit of $k_{\mathrm{eff}}(N)$ at high pressure is given by $k^\infty_{\mathrm{eff}} = k^0_{\mathrm{eff}}(r) - rk_{\mathrm{sat}}$. The possibility to calculate k_{eff} for other low concentrations of c-C_4F_8O is not explored in this work. However, k_{eff} is calculated at different pressures, between 0.1 kPa and 100 kPa in the mixtures of 0.6% c-C_4F_8O in N_2 and 0.5% c-C_4F_8O in CO_2. The calculated k_{eff} are shown in figures 12(a) and (b). The limits of k_{eff} at low and high pressures, k^0_{eff} and k^∞_{eff}, are shown as well. It is instructive to visualize the evolution of $k_{\mathrm{eff}}(N)$ in figure 12, because it makes the link between the (low pressure) beam and (high pressure) swarm results. Towards low gas pressures, the calculated effective ionization rate $k_{\mathrm{eff}}(N)$ approaches k^0_{eff} that was calculated from the beam cross sections with equation (5). This is expected, since the model was constructed based on the beam data. However, it can be seen that at pressures as low as a few millibar, three-body attachment is already significant. The calculations of k_{eff} at high pressures, in particular the limit k^∞_{eff}, can be of interest for instance for high voltage insulation applications, where pressures of a few bars are used.

4.3. Discussion

As the electron kinetics scheme identified with the beam study fails to explain attachment in c-C_4F_8O at superior gas pressure in the swarm experiment, a three-body attachment scheme was introduced. This model explains the strong pressure dependence of the effective ionization rate observed in

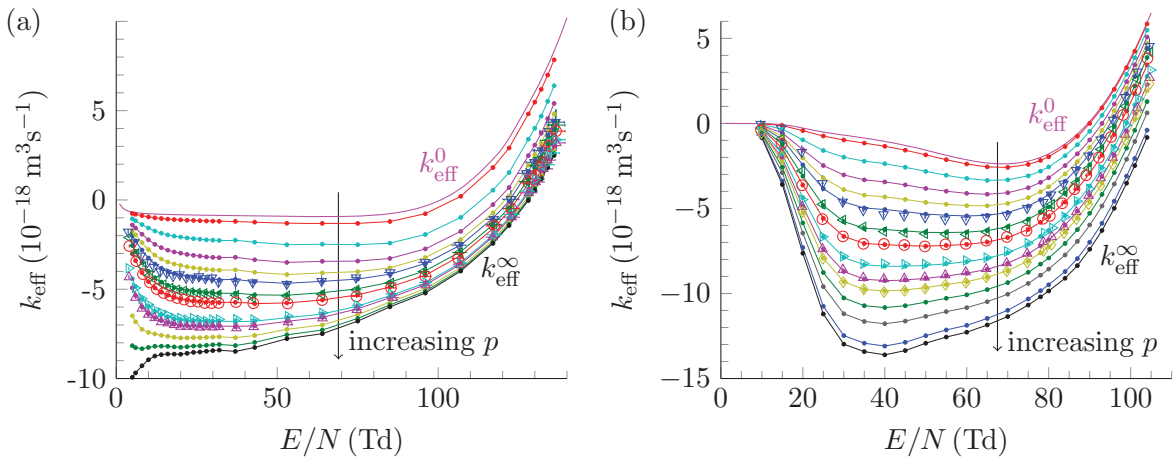

Figure 12. Measured and calculated effective ionization rate coefficient as a function of E/N. (a) In the mixture 0.6% c-C_4F_8O in N_2 for the pressures $p \to 0$ (k^0_{eff}), $p = 0.1$, 0.5, 1, 1.5, 2, 3, 4, 8, 10, 20 and 50 kPa, and $p \to \infty$ (k^∞_{eff}). (b) In the mixture 0.5% c-C_4F_8O in CO_2 for the pressures $p \to 0$ (k^0_{eff}), $p = 0.1$, 0.5, 1, 1.5, 2, 3, 4, 6, 8, 10, 15, 25 and 100 kPa, and $p \to \infty$ (k^∞_{eff}).

the swarm study. Similar dependencies of the effective ionization rate on the gas pressure or temperature were observed in numerous other gases [34, 40, 41] and were attributed to the occurrence of three-body electron attachment. Thus the occurrence of three-body attachment to c-C_4F_8O is quite plausible. However, three-body attachment could occur with a more complex scheme than the one presently used. Some models were proposed for instance involving ion clusters [42]. In the present work, the kinetics scheme was chosen to be as simple as possible but consistent with the measured data. Thus, it should be seen only as a first attempt to explain the complex electron attachment mechanism to c-C_4F_8O, and a useful guess tool for extending the present data to higher pressures. An analysis of the ion composition produced in the swarm experiment would be a possible approach to gain more information on the attachment mechanism to c-C_4F_8O.

5. Conclusion

In conclusion, we have measured electron attachment properties of c-C_4F_8O in two different environments. The electron attachment and ionization cross sections of c-C_4F_8O were obtained using a beam experiment. The effective ionization rates in the diluted mixtures of c-C_4F_8O in buffer gases in the pressure range 2–10 kPa were obtained using a swarm experiment. The pressure difference between the two experiments—approximately five orders of magnitude—leads to dramatic changes in attachment properties of c-C_4F_8O. Therefore, a three-body attachment model was proposed. This model explains the increased electron attachment observed in the swarm experiment, provides a direct link between low-pressure and high-pressure data, and predicts the effective ionization rate of c-C_4F_8O mixtures with N_2 and CO_2 at conditions beyond the range of the present experiments.

Acknowledgments

Thanks to N Aleksandrov for kind explanations. This work is financially supported by GE Grid (Switzerland) GmbH, Pfiffner AG and ABB Switzerland. We also gratefully acknowledge the Swiss National Science Foundation (SNSF Project No. PZ00P2_132357) and the Scientific Exchange Programme (SCIEX Project 12.224).

References

[1] Artuso M *et al* 2006 Performance of a C_4F_8O gas radiator ring imaging Cherenkov detector using multi-anode photomultiplier tubes *Nucl. Instrum. Methods Phys. Res.* A **558** 373

[2] Kim K J *et al* 2004 Global warming gas emission during plasma cleaning process of silicon nitride using c-C_4F_8O/O_2 chemistry with additive Ar and N_2 *J. Vac. Sci. Technol.* B **22** 483

[3] Myhre G *et al* 2013 Anthropogenic and natural radiative forcing *Climate Change 2013: the Physical Science Basis. Contribution of Working Group I to the 5th Assessment Report of the Intergovernmental Panel on Climate Change* ed T F Stocker *et al* (Cambridge: Cambridge University Press) p 731

[4] Robson R E, Nicoletopoulos P, Li B and White R D 2008 Kinetic theoretical and fluid modelling of plasmas and swarms: the big picture *Plasma Sources Sci. Technol.* **17** 075201

[5] Pancheshnyi S *et al* 2012 The LXCat project: electron scattering cross sections and swarm parameters for low temperature plasma modeling *Chem. Phys.* **398** 148–53

[6] Christophorou L G 1988 Insulating gases *Nucl. Instrum. Methods* A **268** 424–33

[7] Franck C M, Dahl D A, Rabie M, Haefliger P and Koch M 2013 An efficient procedure to identify and quantify new molecules for insulating gas mixtures *Contrib. Plasma Phys.* **54** 3–13

[8] Hagelaar G J M and Pitchford L C 2005 Solving the Boltzmann equation to obtain electron transport coefficients and rate coefficients for fluid models *Plasma Sources Sci. Technol.* **14** 722

[9] Biagi S F 1999 Monte Carlo simulation of electron drift and diffusion in counting gases under the inluence of electric and magnetic fields *Nucl. Instrum. Methods* A **421** 234–40

[10] Rabie M and Franck C M 2016 METHES: a Monte Carlo collision code for the simulation of electron transport in low temperature plasmas *Comput. Phys. Commun.* **203** 268–77

[11] Christophorou L G (ed) 1984 *Electron-Molecule Interactions and their Applications* vol 1 (New York: Academic)

[12] Compton R N, Christophorou L G, Hurst G S and Reinhardt P W 1966 Nondissociative electron capture in complex molecules and negative-ion lifetimes *J. Chem. Phys.* **45** 4634

[13] Christophorou L G and Hunter S R 1984 Electrons in dense gases *Swarms of Ions and Electrons in Gases* ed W Lindinger *et al* (New York: Springer)

[14] Gallagher J W, Beaty E C, Dutton J and Pitchford L C 1983 An annotated compilation and appraisal of electron swarm data in electronegative gases *J. Phys. Chem. Ref. Data* **12** 109

[15] Dahl D A, Rabie M, Haefliger P and Franck C M 2014 Electron attaching properties of c-C_4F_8O derived from swarm parameter measurements in buffer gases *Conf. Paper Gas Discharges Orleans* (July, 2014)

[16] Fedor J, May O and Allan M 2008 Absolute cross sections for dissociative electron attachment to HCl, HBr, and their deuterated analogs *Phys. Rev.* A **78** 032701

[17] May O, Fedor J and Allan M 2009 Isotope effect in dissociative electron attachment to acetylene *Phys. Rev.* A **78** 012706

[18] Janečková R, May O, Milosavljević A and Fedor J 2014 Partial cross sections for dissociative electron attachment in tetrahydrofuran reveal a dynamics-driven rich fragmentation pattern *Int. J. Mass. Spetrom.* **163** 365–6

[19] May O, Fedor J, Ibnescu B C and Allan M 2008 Absolute cross sections for dissociative electron attachment to acetylene and diacetylene *Phys. Rev.* A **77** 040701

[20] Janečková R, Kubala D, May O, Fedor J and Allan M 2013 Experimental evidence on the mechanism of dissociative electron attachment to formic acid *Phys. Rev. Lett.* **111** 213201

[21] Straub H C, Renault P, Lindsay B G, Smith K A and Stebbings R F 1995 Absolute partial and total cross sections for electron-impact ionization of argon from threshold to 1000 eV *Phys. Rev.* A **52** 1115

[22] Janečková R, Kočišek J and Fedor J Unusually long-lived transient negative ion of c-C_4F_8O in preparation

[23] Gstir B, Hanel G, Fedor J, Probst M, Scheier P, Mason N J and Märk T D 2002 Electron impact ionization studies for SF_5CF_3 *J. Phys. B: At. Mol. Opt. Phys.* **35** 2567

[24] Hanel G, Fedor J, Gstir B, Probst M, Scheier P, Märk T D, Tegeder P, Mason N J 2002 Electron impact ionization studies for Cl_2O monomers and dimers *J. Phys. B: At. Mol. Opt. Phys.* **35** 589

[25] LXCAT Plasma Data Exchange Project www.lxcat.net

[26] Biagi-v8.9 database www.lxcat.net, retrieved 18/03/2014

[27] Phelps database www.lxcat.net, retrieved 27/06/2014

[28] SIGLO database www.lxcat.net, retrieved 05/07/2014

[29] Blevin H A, Fletcher J and Hunter S R 1985 Electron-velocity distribution functions in gases: the influence of anisotropic scattering and electron nonconservation by attachment and ionization *Phys. Rev.* A **31** 2215

[30] Bordage M C, Segur P and Chouki A 1996 Determination of a set of electron impact cross sections in tetrafluoromethane consistent with experimental determination of swarm parameters *J. Appl. Phys* **80** 1325

[31] Phelps A V and Pitchford L C 1985 Anisotropic scattering of electrons by N_2 and its effect on electron transport *Phys. Rev.* A **31** 2932

[32] Pitchford L C *et al* 2013 Comparisons of sets of electron-neutral scattering cross sections and swarm parameters in noble gases: I. Argon *J. Phys. D: Appl. Phys.* **46** 334001

[33] Dahl D A, Teich T A and Franck C M 2012 Obtaining precise electron swarm parameters from a pulsed Townsend setup *J. Phys. D: Appl. Phys.* **45** 485201

[34] Chachereau A, Rabie M and Franck C M 2016 Electron swarm parameters of the hydrofluoroolefine HFO1234ze *Plasma Sources Sci. Technol.* **25** 045005

[35] ETHZ database www.lxcat.net

[36] Yamaji M, Nakamura Y 2003 Measurements of electron transport coefficients in the 0.468% and 4.910% c-C_4F_8/Ar mixtures and pure c-C_4F_8 *J. Phys. D: Appl. Phys.* **36** 640–4

[37] Long W H Jr, Bailey F W and Garscadden A 1976 Electron drift velocities in molecular-gas-rare-gas mixtures *Phys. Rev.* A **13** 471

[38] Petrovic Z L, Crompton R W and Haddad G N 1984 Model calculations of negative differential conductivity in gases *Aust. J. Phys.* **37** 23

[39] Vrhovac S B and Petrovic Z L 1996 Momentum transfer theory of nonconservative charged particle transport in mixtures of gases: general equations and negative differential conductivity *Phys. Rev.* E **53** 4012

[40] Aleksandrov N L 1988 Three-body electron attachment to a molecule *Usp. Fiz. Nauk* **154** 177–206

[41] Christophorou L G, Mathis R A, Hunter S R and Carter J G 1988 Effect of temperature on the uniform field breakdown strength of electronegative gases *J. Appl. Phys.* **63** 52

[42] Hunter S R, Christophorou L G, McCorkle D L, Sauers I, Ellis H W and James D R 1983 Anomalous electron attachment properties of perfluoropropylene (1-C3F6) and their effect on the breakdown strength of these gases *J. Phys. D: Appl. Phys.* **16** 573–80